Article:
Xia, Y., Xu, R., Ye, S. et al. (4 more authors) (2023) Microfluidic formulation of curcumin-loaded multiresponsive gelatin nanoparticles for anticancer therapy. ACS Biomaterials Science & Engineering, 9 (6). pp. 3402-3413. ISSN 2373-9878

https://doi.org/10.1021/acsbiomaterials.3c00318

ACS Biomaterials SCIENCE & ENGINEERING

pubs.acs.org/journal/abseba

Article

Microfluidic Formulation of Curcumin-Loaded Multiresponsive Gelatin Nanoparticles for Anticancer Therapy

Yu Xia,[‖] Ruicheng Xu,[‖] Siyuan Ye, Jiaxuan Yan, Piyush Kumar, Peng Zhang, and Xiubo Zhao*

Cite This: *ACS Biomater. Sci. Eng.* 2023, 9, 3402−3413

Read Online

ACCESS | Metrics & More | Article Recommendations | Supporting Information

ABSTRACT: Current anticancer research shows that a combination of multiple treatment methods can greatly improve the killing of tumor cells. Using the latest microfluidic swirl mixer technology, combined with chemotherapy and photothermal-ablation therapy, we developed multi-responsive targeted antitumor nanoparticles (NPs) made of folate-functionalized gelatin NPs under 200 nm in size and with encapsulated CuS NPs, Fe_3O_4 NPs, and curcumin (Cur). By exploring gelatin's structure, adjusting its concentration and pH, and fine-tuning the fluid dynamics in the microfluidic device, the best preparation conditions were obtained for gelatin NPs with an average particle size of 90 ± 7 nm. The comparative targeting of the drug delivery system (DDS) was demonstrated on lung adenocarcinoma A549 cells (low level of folate receptors) and breast adenocarcinoma MCF-7 cells (high level of folate receptors). Folic acid helps achieve targeting and accurate delivery of NPs to the MCF-7 tumor cells. The synergistic photothermal ablation and curcumin's anticancer activity are achieved through infrared light irradiation (980 nm), while Fe_3O_4 is guided with an external magnetic field to target gelatin NPs and accelerate the uptake of drugs, thus efficiently killing tumor cells. The method described in this work is simple, easy to repeat, and has great potential to be scaled up for industrial production and subsequent clinical use.

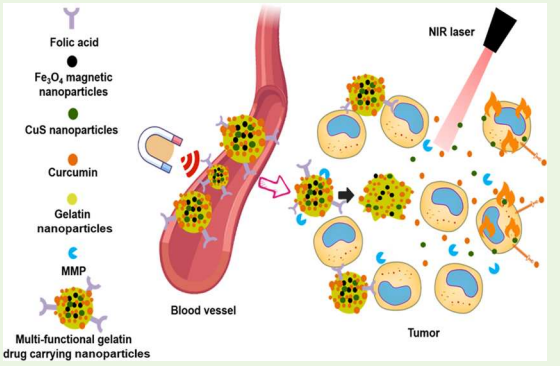

KEYWORDS: *microfluidics, nanomedicine, anticancer therapy, targeted drug delivery, gelatin nanoparticles, photothermal ablation*

1. INTRODUCTION

Cancer is a major disease that seriously affects human life and health.[1−3] At present, cancer treatment includes surgical resection, radiotherapy, and chemotherapy,[4] and in recent years, gene therapy,[5,6] cell therapy,[7,8] photodynamic therapy,[9−11] and photothermal-ablation therapy.[12−14] Each method has its own pros and cons, and anticancer approaches combining two or more methodologies have been shown to be much more effective.[15,16] Therefore, therapeutic formulations combining multiple treatment methods are more promising for the future of anticancer therapies.

In the past three decades, the development of nanotechnology and its application in medicine (nanomedicine) has evolved rapidly. Nanodrug delivery systems (DDSs) have shown strong anticancer effects due to their ability to prevent the degradation of active pharmaceutical ingredients (APIs), being targeted, controlled release, high bioavailability, low toxicity, and side effects.[17−21] However, preparing such DDSs is challenging. It is of far-reaching significance to design nanoformulations with stable structures and controllable nanoparticle (NP) sizes.[22] NPs with sizes less than 200 nm are easier to reach the tumor site due to the enhanced permeability and retention (EPR) effect. Small NPs also have the advantage of being able to easily enter cells through endocytosis. On the other hand, the controlled release of anticancer drugs can be achieved through the fine-tuning of the chemical properties of constituent materials used in NP fabrication. At present, commonly used biomaterials for nanodrug formulations include lipids (e.g., liposomes, lipid nanoparticles),[23−25] polymers (e.g., PLGA, PLA, chitosan, alginate),[26] and proteins (e.g., collagen, gelatin, silk, albumin).[21,27−30] Gelatin is a natural protein that can be obtained by partial acid or alkali hydrolysis, thermal degradation, or enzymatic degradation of structural animal collagen.[31] Compared with collagen, gelatin does not express antigenicity *in vivo* and is easy to dissolve in an aqueous solution.[14] Gelatin has become a highly versatile platform for extensive applications in the biomedical field due to its good biocompatibility, biodegradability, nontoxicity, non-antigenicity, and structural plasticity.

Stimulation-responsive nano-DDSs perform significantly better than conventional DDSs and can respond to specific stimuli at the disease/tumor site, leading to changes in their

Received: March 12, 2023
Accepted: April 24, 2023
Published: May 4, 2023

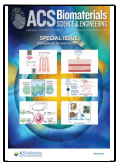

physical and chemical properties and decomposition or fragmentation.[32] Copper sulfide (CuS) is an inorganic compound, and its NPs have excellent optical and thermal properties. The therapeutic principle behind using CuS NPs is that they can have adjustable absorption peaks in the near-infrared region (700−1100 nm), within which the normal human tissues do not have any absorption peaks, and thus causing no background interference. CuS NPs can increase the temperature in the tumor microenvironment by converting the absorbed infrared light into heat, thereby killing cells. However, because of the complexity of *in vivo* clinical treatment, it is difficult to achieve precisely targeted treatment with only a single NP species, as it is easy for the CuS NPs to flow through the entire body with blood.[33] Therefore, we have added superparamagnetic iron oxide (Fe_3O_4) NPs, which can be easily guided by an external magnetic field. In addition, based on the magnetocaloric function of magnetic NPs (MNPs), thermally responsive drug release can also be controlled by the controlled fluctuation of the applied external magnetic field.

Microfluidics can provide precise control and rapid mixing and has shown great potential in developing new NPs with controllable sizes and compositions.[4,34,35] The commonly used microfluidic technologies include the T-junction, hydrodynamic flow focusing, staggered herringbone, toroidal mixer, multi-inlet vortex mixers, etc.[34,36] Recently, a newly developed swirl mixer has shown great potential for the fabrication of lipid NPs and polymer NPs at a large scale with high uniformity.[24] It has been used for the formulation of silk NPs,[29,37] ZIF-8 NPs,[35] curcumin,[38] doxorubicin,[39] and Ansamitocin P-3[25] loaded liposomes for anticancer therapy. The swirl mixer can achieve a high flow rate of 320 mL/min with a mixing time of 0.1 ms, achieving a PDI of 0.06 ± 0.02 for liposome formulation,[38] demonstrating its great potential for industrial application of nanoformulation.

In this work, the swirl mixer was used to prepare the gelatin NPs with excellent stability for over 2 weeks. Gelatin was functionalized with folic acid (for targeting) and dissolved in DI-water as the aqueous phase, and ethanol or ethanol with Tween-20 was used as the organic phase (antisolvents). CuS and MNPs were blended into the aqueous phase, and curcumin was blended into the organic phase for the fabrication of drug/CuS/MNP-loaded gelatin NPs. We studied the effects of gelatin concentration, solution pH, the composition of antisolvent, the flow rate ratio (FRR), and the total flow rate (TFR) to explore the conditions for controlling particle size and polydispersity. The optimum size was around 90 nm with a PDI <0.1. The curcumin/CuS/MNP-loaded gelatin NPs showed great response to the near-infrared light and magnetic field. The MNPs facilitated cellular uptake of the gelatin NPs, and folic acid enhanced the cancer cell-targeting effect. CuS inside the gelatin NPs enhanced its anticancer effect through near-infrared light irradiation. Overall, the current work demonstrated a promising strategy for the microfluidic fabrication of multicomponent-loaded gelatin NPs for anticancer therapy.

2. EXPERIMENTAL SECTION

2.1. Materials. Gelatin type B was obtained from Aladdin Chemistry Co. Ltd. (Shanghai). Carbonate−bicarbonate (CB) buffer and D_2O were obtained from Beijing InnoChem Science & Technology Co. Ltd. $CuCl_2{\cdot}2H_2O$, poly(vinylpyrrolidone), $Na_2S{\cdot}9H_2O$, sodium citrate ($C_6H_5Na_3O_7$), folic acid, *N*-hydroxysuccinimide (NHS), 1-ethyl-3-(3-dimethylaminopropyl)carbodiimide (EDC), 1-(3-dimethylaminopropyl)-3-ethylcarbodiimide hydrochloride, dimethyl sulfoxide (DMSO), 4% paraformaldehyde fixing solution, 0.25% trypsin, and glutaraldehyde were purchased from Sinopharm Chemical Reagent Co., Ltd. Dulbecco's modified Eagle's medium (DMEM), fetal bovine serum (FBS), and penicillin/streptomycin were obtained from Gibco (Thermos Fisher Scientific). 3-(4,5-Dimethylthiazol-2-yl)-2,5-diphenylte-trazolium bromide (MTT), 4′,6-diamidine-2′-phenylindole dihydro-chloride (DAPI), 2′-(4-ethoxyphenyl)-5-(4-methyl-1-piperazinyl)-2,5′-bi-1*H*-benzimidazole, trihydrochloride (Hoechst 33342), and propidium iodide (PI) were purchased from Beijing Solarbio Bio-Tech Co. Ltd. (China). All other reagents used in this research were of analytical grade.

2.2. Preparation of CuS Nanoparticles. A total of 8.525 mg of $CuCl_2{\cdot}2H_2O$ and 20 mg of trisodium citrate were dissolved in 45 mL of deionized water and stirred at 800 rpm for 5 min. The temperature was adjusted to 90 °C before 5 mL of Na_2S (2 mg/mL) solution was added and stirred for another 15 min to obtain dark green CuS NPs. The reaction was then stopped, and the solution was cooled down to room temperature. The larger particles were removed with a 0.22 μm filter.

2.3. Preparation of Fe_3O_4 Nanoparticles. The mature oleic acid preparation method was used to prepare Fe_3O_4 NPs.[39−41] Briefly, 2.824 g of iron acetylacetonate, 6.4 g of cetylamine, 6.4 mL of oleic acid, and 60 mL of diphenyl ether were placed in a 150 mL three-port flask, slowly heated to 260 °C, and stabilized for 10 min under constant stirring. The reaction was refluxed for 2 h, after which the reaction was stopped and cooled down to room temperature before 120 mL of absolute ethanol was added and sonicated for 15 min. The solution was then centrifuged at 12,000 rpm for 20 min to remove the supernatant. The pellet was dispersed in 40 mL hexane with 0.4 mL of oleic acid and kept in a 4 °C refrigerator.

2.4. Gelatin Modification. The grafting method developed by Zhang et al.[42] was optimized before use. Briefly, 120 mg of folic acid (FA), 31.2 mg of NHS, and 42 mg of EDC were added to 15 mL of DMSO solution, stirred, and reacted at room temperature overnight to fully activate folic acid. The activated folic acid DMSO solution was added dropwise to 75 mL of deionized water and stirred rapidly, followed by centrifugation at 8500 rpm for 10 min. The supernatant was discarded, and the pellet was washed with water twice before being redissolved with 20 mL of DMSO. Then, 180 mg of gelatin type B was dissolved in 36 mL of CB buffer and heated to 45 °C for 15 min to melt the gelatin. Afterwards, 20 mL of FA−DMSO solution was added dropwise, until the gelatin solution became clear and transparent, and stirred overnight. The reaction product was placed in a 3500 kDa dialysis bag and dialyzed in a 20% DMSO aqueous solution for 48 h before being lyophilized. The folate content was determined according to the literature.[43] The absorption coefficient (ε) of folic acid is 6200 M^{-1} cm^{-1} at 363 nm. The folic acid content of the modified gelatin was calculated using the equation $A = \varepsilon BC$, where A is the absorbance, B is the thickness of the light-absorbing pass length, and C is the concentration of the light-absorbing substance.

2.5. Microfluidic Production of Gelatin Nanoparticles. Modified gelatin was added to water and heated to 45 °C for 30 min to dissolve completely. Gelatin solutions with different concentrations and pHs were used as the aqueous phase. For the organic phase, 100% EtOH, 95% EtOH, and 95% EtOH mixed with 2% Tween-20 were used as antisolvents. The flow rate ratios between the aqueous phase and the organic phase were adjusted to 1:1, 1:5, 1:10, 1:20, and 1:30, respectively. The total flow rates of the two phases were set at 10.5 and 40 mL/min. The two phases were injected into the inlets of the microfluidic device[24,25,29,44] for the preparation of gelatin NPs. The particle size and PDI of the gelatin NPs were recorded to optimize the experimental conditions.

2.6. Microfluidic Preparation of Curcumin-Loaded Multi-responsive Gelatin NPs. Modified gelatin (100 mg), CuS solution (5 mL of 0.1 mg/mL), and Fe_3O_4 (50 μL of 2 mg/mL) were added in a round-bottom flask and heated in a 40 °C water bath for 30 min. The pH of the solution was then adjusted to 11 for use as the aqueous

https://doi.org/10.1021/acsbiomaterials.3c00318
ACS Biomater. Sci. Eng. 2023, 9, 3402−3413

phase. Curcumin was dissolved in a 2% Tween-20−95% EtOH solution at a concentration of 0.5 mg/mL for use as the organic phase. The flow rates of the aqueous and organic phases were kept constant at 0.5 and 10 mL/min, respectively, while being injected into the microfluidic device using a syringe pump (Fusion 4000, Chem XY Inc.). The colloidal solution collected at the end of the device was folic acid-modified gelatin NPs encapsulating CuS, Fe_3O_4, and curcumin (Fe_3O_4/CuS/Cur@GNPs-FA). Afterwards, glutaraldehyde solution (2%) was added for cross-linking the gelatin. The NP solution was shaken for 30 min before being filtered with a 0.22 μm filter and dialyzed with a 10 kDa dialysis bag for 48 h before being stored at 4 °C for future use.

2.7. Drug Encapsulation Efficiency (EE) and Loading Capacity (LC). The encapsulation efficiency and loading capacity of the drug were determined by centrifugation. Briefly, 2 mL of the prepared drug-loaded gelatin NP solution was centrifuged at 12,000 rpm for 1 h, and the supernatant was discarded. Then, 1 mL of concentrated hydrochloric acid was added to the precipitate and ultrasonicated for 2 h. The solution was diluted to 10 mL with pure water, and the absorbance value was measured with an ultraviolet spectrophotometer (TU-1901PC, Shanghai, China) at a wavelength of 425 nm. The mass m_1 of the drug was calculated according to the standard curve. Then, 1 mL of concentrated hydrochloric acid was added to another 2 mL of the solution from the same sample for demulsification. The absorbance value was measured with the same method after dilution to 10 mL. The mass m_2 of the drug was calculated, and the encapsulation efficiency of the drug-loaded NPs was calculated using eq 1. The precipitate (from 2 mL of solution) after centrifugation was dried overnight at 25 °C, and the mass of precipitate m_3 was weighed. The drug loading was calculated according to eq 2.

$$\mathrm{EE\%} = (m_1/m_2) \times 100\% \quad (1)$$

$$\mathrm{LC\%} = (m_1/m_3) \times 100\% \quad (2)$$

2.8. Particle Characterization. Fourier transform infrared (FTIR) spectra of folic acid-grafted gelatin lyophilized powders were recorded using grazing incidence attenuated total reflection Fourier transform infrared (ATR-FTIR) spectroscopy (Nicolet iS 10) in the range of 500−4000 cm^{-1}. The particle size, polydispersity indexes (PDI), and zeta potentials of different formulations were measured by dynamic light scattering (Nano-ZS90, Malvern Zetasizer, U.K.). The morphologies of the NPs were observed through transmission electron microscopy (TEM).

2.9. Drug Release and *In Vitro* Stability. The dynamic dialysis method was used to simulate the release of curcumin from gelatin NPs *in vitro*. Briefly, 2 mL of Fe_3O_4/CuS/Cur@GNPs-FA was placed into dialysis bags (MWCO = 10 kDa). The dialysis bags were incubated in 20 mL of prewarmed PBS solution containing 1.5% Tween-80 and 20% anhydrous EtOH (pH = 5.5 and 7.4) with gentle shaking (120 rpm) at 37 °C. The suitability of this *in vitro*-release media for Cur has been reported previously.[45,46] At specific time points, 2 mL of the released medium was collected and replaced with the same volume of fresh medium. The cumulative amounts of Cur in the 2 mL of samples were determined by ultraviolet (UV) spectrophotometry (TU-1901PC, Shanghai, China) at wavelengths of 425 nm, and their cumulative release was calculated. The test was repeated 3 times, and all data were expressed as the mean ± standard deviation.

The stability of NPs was evaluated in PBS (pH 7.4), NS (stroke-physiological saline solution, 0.9% NaCl), or DMEM medium. In brief, Fe_3O_4/CuS/Cur@GNPs-FA was diluted in the medium (1:10, v/v) and stored at 4 °C for 2, 4, 6, 8, 10, 12, 14, and 16 days. Afterwards, the mean size and PDI were measured at different time points.

2.10. Cell Cultures. HFF-1 (Human foreskin fibroblasts), A549 (Human lung adenocarcinoma cells), and MCF-7 (human breast cancer cells) were purchased from the China Center for Type Culture Collection (Shanghai, China). The cells were cultured in DMEM and added with 10% FBS and 1% penicillin/streptomycin at 37 °C and 5% CO_2 in an incubator.

2.11. *In Vitro* Cytotoxicity Assays. MTT assay was performed on HFF-1, MCF-7, and A549 cells to rule out any NP-induced cytotoxicity. Briefly, the cells were evenly seeded in a 96-well culture plate at a density of 5.0×10^3 cells per well and cultured at 37 °C and 5% CO_2 for 24 h. Subsequently, the cells were treated with free-Cur, Fe_3O_4/CuS/Cur@GNPs, and Fe_3O_4/CuS/Cur@GNPs-FA with different concentrations of Cur (10−100 μg/mL) for 24 h. Different concentrations of blank gelatin, CuS, and Fe_3O_4 were incubated with MCF-7 cells to examine biocompatibility. In addition, to evaluate the photothermal effect of CuS, 980 nm near-infrared (NIR) irradiation at 1.0 W/cm^2 was applied for 5 min. After incubation, MTT solution (10 μL, 5 mg/mL) was added to each well and incubated for another 4 h at 37 °C. Then, the medium was removed and washed with PBS before the addition of 150 μL of DMSO. The absorbance of the solution was measured at 570 nm using a microplate reader (Varioskan LUX, Thermo Fisher) to calculate the percent cell viability. Each treatment was repeated six times in 96-well plates.

2.12. Live/Dead Assay. The live/dead cell staining was used for qualitative analysis of cytotoxicity. MCF-7 cells were seeded on cell culture plates at a density of 5.0×10^5 cells/well and cultured for 24 h. The MCF-7 cells were incubated with curcumin, with its final concentration controlled at 10 μg/mL ($n = 4$). In the NIR (+) group, all cells were irradiated with NIR (1.0 W/cm^2, 5 min) at a wavelength of 980 nm after the cells were cultured with curcumin for 24 h. Cells were washed twice with PBS, followed by incubation with Hoechst 33,342 (2 μg/mL) at 37 °C for 10 min and PI (5 μg/mL) for 20 min. The cell morphology was then observed under a fluorescence microscope (Nikon, Japan, Ti2-U). Blue and red stained cells represent live and dead cells, respectively.

2.13. Cellular Uptake. Curcumin itself has green fluorescence, but the fluorescence is quenched quickly under the fluorescence microscope. In order to assess the cellular uptake, a less toxic dye with green fluorescence, coumarin C6, was used instead of curcumin.[47] MCF-7 cells were cultured for 24 h, and then coumarin C6, Fe_3O_4/CuS/C6@GNPs, and Fe_3O_4/CuS/C6@GNPs-FA were added. The final C6 concentration was controlled at 10 μg/mL, with 4 repeated wells per group. The cells were incubated in an incubator for 2, 4, 8, and 12 h, respectively. Next, the cells were washed, fixed with 4% paraformaldehyde for 10 min, and stained with DAPI (0.1 μg/mL) for 8 min, followed by imaging using a fluorescence microscope. The same method was used to analyze the uptake of Fe_3O_4/CuS/C6@GNPs and Fe_3O_4/CuS/C6@GNPs-FA with and without magnetization, respectively.

2.14. Flow Cytometry. Flow cytometry was used for the quantitative determination of fluorescent drug uptake. MCF-7 cells were seeded on a 6-well plate at a density of 1×10^6 cells/mL and cultured overnight for 24 h. Coumarin C6, Fe_3O_4/CuS/C6@GNPs, and Fe_3O_4/CuS/C6@GNPs-FA were added to the wells, respectively, and the concentration of coumarin C6 was controlled at 1 μg/mL. Three repeats were set up in each group, and DMEM medium (containing cells) was used as the control group. After incubation for 2, 4, 8, and 12 h, cells were washed three times with PBS (pH 7.4) to remove unbound drug and harvested separately by trypsin digestion. The internalization efficiencies of the cells were analyzed using flow cytometry (BD Biosciences, Accuri C5). Data from a total of 10,000 events were acquired for each sample, and the mean fluorescence intensity of C6 in the cells was analyzed using FlowJo software. The same method was used to analyze the uptake of Fe_3O_4/CuS/C6@GNPs and Fe_3O_4/CuS/C6@GNPs-FA with and without magnetization, respectively.

2.15. Statistical Analysis. All values in this study were expressed as means ± SD (standard deviation). Differences among groups were analyzed using one-way analysis of variance (ANOVA) with GraphPad Prism 9.0 software. Statistical differences were considered significant at $^{****}P < 0.0001$; $^{***}P < 0.001$; $^{**}P < 0.01$; and $^{*}P < 0.05$.

https://doi.org/10.1021/acsbiomaterials.3c00318
ACS Biomater. Sci. Eng. 2023, 9, 3402−3413

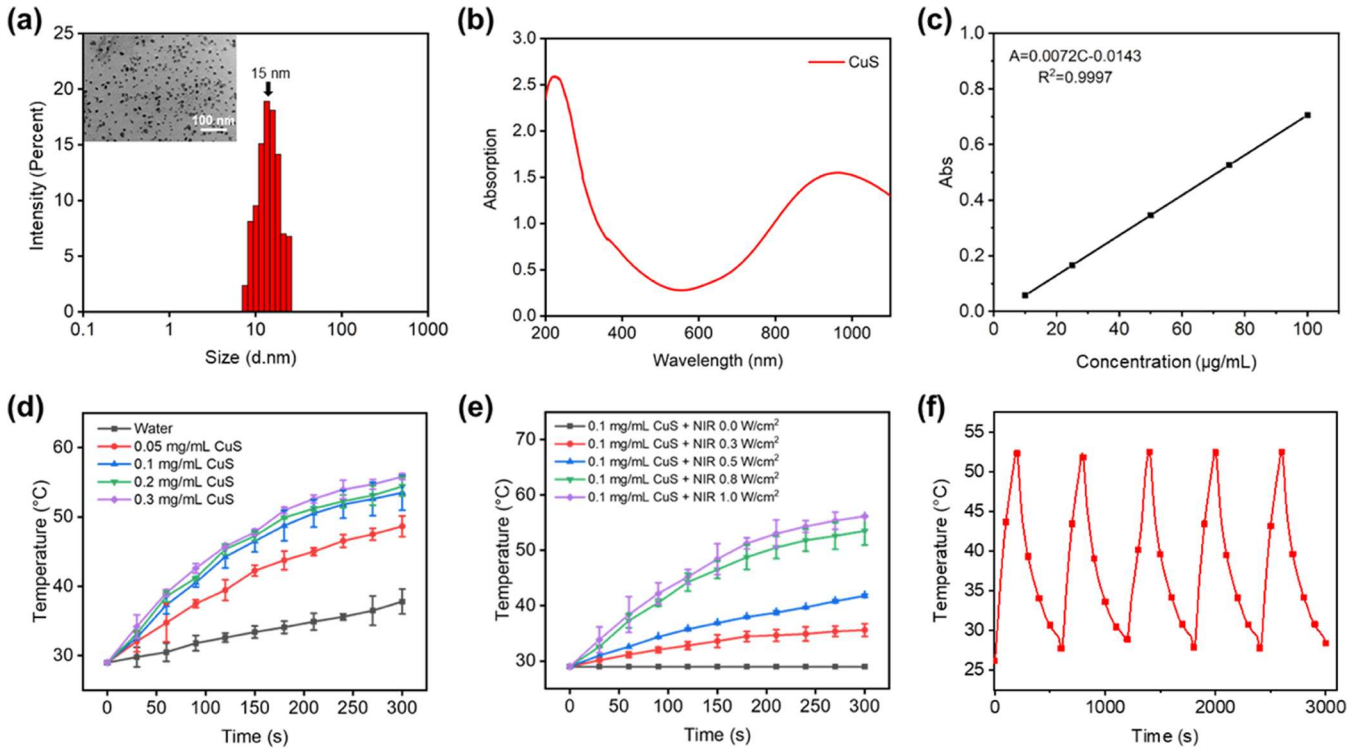

Figure 1. Characterization of CuS nanoparticles. (a) TEM image of CuS with size distribution. (b) UV−vis−NIR absorption spectra of CuS. (c) Standard equation of CuS solution in the concentration range of 0.1−1 mg/mL. (d) Temperature change with CuS concentrations under infrared light irradiation at 980 nm and a power of 1.0 W/cm^2. (e) Temperature change over time of CuS solutions (0.1 mg/mL) with different irradiation powers (0−1 W/cm^2) at 980 nm. (f) Continuous heating and cooling curve of a CuS solution (1 W/cm^2).

3. RESULTS AND DISCUSSION

3.1. Characterization of Modified Gelatin. EDC and NHS were used as coupling agents for gelatin and folic acid.[48] Notably, folic acid has two carboxylic groups denoted as α and γ, and it has been recognized that γ is more reactive than α carboxyl.[49,50] When the amount of folic acid is small, most of the γ carboxyl groups involve in grafting and react with the primary amine groups in gelatin to form amide bonds. The infrared spectrum of free folic acid has three characteristic peaks at 1601, 1687, and 1487 cm^{-1}. Figure S1a shows the FTIR spectrum of the lyophilized powder of folic acid-grafted gelatin recorded in the range of 500−4000 cm^{-1}. A distinct characteristic peak between 1650 and 1690 cm^{-1} confirmed the formation of an amide bond between gelatin and folic acid.[51]

There are many characteristic peaks in the hydrogen spectrum of gelatin type B; for example, the methyl resonance of leucine, valine, and isoleucine corresponds to 0.76 ppm, and that of aspartic acid corresponds to 2.84 ppm.[52] After lyophilizing, 10 mg of folic acid gelatin powder was added to 60 μL of deuterium oxide (D_2O), and the ^{1}H NMR spectrum was measured after heating to 45 °C for 10 min. Figure S1b shows two additional peaks at 1.79 and 2.57 ppm for folic acid-grafted gelatin due to the grafting of folic acid, while the shoulder peak at 7.16 ppm was a characteristic peak due to the aromatic proton resonance of gelatin type B and folic acid.[51] The above results indicate that folic acid was successfully grafted on gelatin. The folate content was determined according to the literature[43] and was found to be 56.3 ± 1.4% in the modified gelatin.

3.2. Characterization of CuS Nanoparticles. TEM and dynamic light scattering (DLS) results showed that the particle size of the CuS NPs prepared in this study was about 15 nm (Figure 1a). The UV-NIR absorption curve (Figure 1b) demonstrated that the maximum absorption wavelength was 980 nm for the prepared CuS NPs, which is consistent with the previous report.[53] Therefore, the prepared CuS NPs can be used for photothermal-ablation therapy. Figure 1c shows the standard curve of absorbance for the CuS NP aqueous solution. Linear regression was performed on the absorbance value and the CuS NP concentration, and the linear equation obtained was: $A = 0.0072C - 0.0143$ ($R^2 = 0.9997$), where A represents absorbance; C represents the concentration of CuS in μg/mL; and R represents the fitting correlation coefficient. The temperature of the CuS NP suspension increased rapidly under the irradiation of 980 nm NIR light (1.0 W/cm^2), and the higher the concentration, the faster the temperature raised (Figure 1d) with 0.1, 0.2, and 0.3 mg/mL of CuS solutions reaching the killing temperature of cancer cells (>50 °C) within 300 s of irradiation. To avoid damage to normal tissues, 0.1 mg/mL was chosen as the optimal concentration for this study. The power of the NIR light had a significant effect on the photothermal effect of the CuS NPs (Figure 1e). Under the NIR irradiation at 1.0 W/cm^2, the temperature of the CuS NP solution reached 53.5 °C within 300 s, and therefore, it was chosen as the optimal irradiation power. The stability of the photothermal effect of CuS NPs was investigated by applying five heating−cooling cycles (Figure 1f). The CuS NPs exhibited a repeated rise and fall in temperature during each irradiation process. The photothermal effect of CuS NPs is realized via the d−d energy band transition of Cu^{2+}, which can provide stable and sustainable energy conversion under repeated NIR light irradiation even in a complex *in vivo* environment.

https://doi.org/10.1021/acsbiomaterials.3c00318
ACS Biomater. Sci. Eng. 2023, 9, 3402−3413

3.3. Characterization of Fe_3O_4 Nanoparticles. The morphology of the Fe_3O_4 NPs was observed using a TEM and a scanning electron microscope (SEM). The prepared magnetic NPs (MNPs) were spherical with a uniform size of 12 ± 3 nm (Figure S2a). The characteristic peaks of the X-ray diffraction (XRD) pattern of the prepared MNPs were consistent with the Fe_3O_4 standard diffraction card (19−0629) (Figure S2b). Taking characteristic peaks (220), (310), (400), (422), (511), and (440) into the Debye−Scherrer formula, the average particle size of MNPs was calculated as 12 nm, consistent with the TEM results. The MNPs showed a large infrared absorption peak at 585 nm (Figure S2c), which was consistent with the literature.[54] Figure S2d shows the magnetization results of Fe_3O_4. The saturation magnetic strength of the MNPs was 76 emu/g, indicating that they are superparamagnetic materials.

3.4. Preparation of Gelatin NPs. *3.4.1. Effect of Modified Gelatin Concentration on the Size and PDI of Gelatin NPs.* As shown in Table 1, the gelatin concentration had a significant effect on the size and PDI of the final gelatin NPs. The NP size and PDI were, respectively, 116 nm and 0.15 at 1% gelatin concentration and 85 nm and 0.09 at 2% gelatin concentration. The NPs became slightly bigger at higher concentrations of gelatin. Therefore, 2% was selected as the optimal gelatin concentration in this study.

Table 1. Effects of Concentration, pH, Antisolvent, Flow Rate Ratio, and Total Flow Rate on Gelatin Nanoparticles

	parameters	mean size (nm)	PDI
effects of gelatin concentration	1%	116	0.15
	2%	85	0.09
	3%	108	0.06
	5%	102	0.07
effects of pH	5.8	1009	0.46
	11	85	0.07
effects of solvent	EtOH	138	0.25
	95% EtOH	103	0.23
	2% Tween-20 in 95% EtOH	85	0.05
effects of flow rate ratio (FRR) (A/S)	1:1	112	1
	1:5	187	0.07
	1:10	205	0.06
	1:20	117	0.06
	1:30	215	0.42
effects of total flow rate (TFR) mL/min	1.05	112	0.11
	10.5	85	0.09
	21	90	0.09
	31.5	90	0.07
	42	97	0.05

3.4.2. Effect of pH on Modified Gelatin NPs. The isoelectric point of gelatin type B is between 4.8 and 5.0,[55] and within this range, gelatin exhibits low viscosity and low swelling rate, which leads to cross-linking between different gelatin NPs.[55] Therefore, in this study, a suitable pH was selected to ensure that the surface of gelatin NPs has an appropriate amount of charge so that the NPs are repulsive towards each other, which helps in maintaining good stability. In accordance with previous work,[51] the pH values of 5.8 and 11 were selected, respectively. As shown in Table 1, when pH was 5.8, the particle size of the prepared NPs exceeded 1000 nm, and their PDI was greater than 0.4, whereas the size of the NPs prepared at pH 11 was less than 100 nm in size, and their PDI was less than 0.1. Therefore, pH 11 was chosen as the optimal pH value in this study.

3.4.3. Effect of the Antisolvent. The antisolvent also showed different effects on NP formation. Tween, as a nonionic surfactant commonly used in drug delivery systems, can effectively reduce the size of NPs.[56] The principle of its action is the reduction of mutual cohesion between gelatin particles, thus maintaining the stability of the gelatin NP solution and preventing large-scale flocculation. In addition, a reasonable amount of Tween can compete for water molecules against gelatin in the solution so that the water-deficient edge of the gelatin chain tends to shrink at both ends and agglomerate into NPs.[57] As shown in Table 1, the particle size of the gelatin NPs prepared by using the 95% ethanol solution containing 2% Tween-20 as the organic phase was much smaller (at 90 nm with 0.05 PDI) than that of the gelatin NPs prepared by absolute ethanol and 95% ethanol. Therefore, in this study, 95% ethanol solution containing 2% Tween-20 was selected as the organic phase for the preparation of modified gelatin NPs.

3.4.4. Effects of the Two-Phase Flow Rate Ratio (FRR) and Total Flow Rate (TFR). The FRR and TFR of the aqueous phase and organic phase had significant effects on the particle size and PDI of NPs (Table 1). When the FRR (A/S) was 1:20, the particle size and PDI of the prepared gelatin NPs were relatively smaller. Although the particle size was the smallest when the FRR (A/S) was 1:1, the PDI of the prepared gelatin NPs turned out to be 1. Therefore, the optimal FRR of the aqueous phase to the organic phase was chosen to be 1:20 in this study. When the FRR was 1:20 and the TFR was greater than 10.5 mL/min, the size of the prepared gelatin NPs was relatively smaller (∼90 nm) and the PDI was less than 0.1. The TFR of 10.5 mL/min was selected for the preparation of gelatin NPs with uniform size and good polydispersity for the following study.

The particle size and preparation time were compared with conventional microsphere preparation methods, such as the water-in-oil emulsion (W/O) method and the emulsion cross-linking method (Table 2). It can be seen from the table that in addition to the preparation using microfluidics, other conventional preparation methods are insufficient to achieve nanoscale gelatin particles, and most of the prepared particles are in the range of 10−50 μm, which are not suitable for use as nanocarriers for drug delivery. It is worth mentioning that the swirl mixer used in this study can prepare gelatin NPs with sizes less than 200 nm within 30 min (Table 1), which has not been reported yet. The preparation time (0.5 h) also includes the curing time of gelatin NPs, as the microfluidic fabrication time only takes a few minutes. Therefore, considering both the size of the NPs and the preparation time, the swirl mixer microfluidic technology has unique advantages and is more suitable for large-scale continuous industrial production.

3.5. Characterization of Drug-Loaded Gelatin Nanoparticles. Particle sizes, PDI, ζ-potentials, encapsulation efficiency (EE), and loading capacity (LC) of curcumin, CuS, and Fe_3O_4 were measured as shown in Figures S3−S6. The entrapment efficiency varied (between 30 and 80%) with the different Cur concentrations studied (1−5 mg/mL). The highest entrapment efficiency was obtained at the Cur concentration of 2 mg/mL (Figure S3). The loading efficiency and particle size increased with the increase in studied Cur concentrations, and the loading efficiency plateaued at 25%,

https://doi.org/10.1021/acsbiomaterials.3c00318
ACS Biomater. Sci. Eng. 2023, 9, 3402−3413

Table 2. Comparison of Different Preparation Methods of Gelatin Particles

preparation methods	size	preparation time (h)	refs
microfluidic method (swirl mixer)	180 ± 10 nm	<0.5	this work
microfluidic method (tapering capillaries)	between tens of microns and hundreds of microns		58
emulsion method	5 μm	>6	59
emulsion method	12 ± 3 μm	0.75	60
water-in-oil emulsion method	13 ± 3 μm	49	61
water-in-oil emulsion method	16 ± 4 μm	48	62
water-in-oil emulsion method	25 μm	0.75	63
water-in-oil emulsion method	40−50 μm	22	64
water-in-oil emulsion method	50 ± 18 μm	49	60, 65
oil-in-water-in-oil emulsion method	5−40 μm	>8	65, 66
emulsion cross-linking method	613 nm	3	67
electrohydrodynamic atomization	0.5 μm	>1	59, 68

while the ζ-potential decreased (to −20 mV) with the increasing Cur concentration, indicating the increased drug encapsulation. At the highest entrapment efficiency, the size of the nanoparticle was 120 nm with a narrow size distribution (PDI <0.2). When the concentration of CuS was 0.125 mg/mL, the entrapment efficiency was the highest (75%) (Figure S4) with the loading efficiency of around 2%. The particle size increased with the increase in studied CuS concentrations, with the size (200 nm) distribution (0.2) being the narrowest at the concentration of 0.125 mg/mL. When the concentration of Fe_3O_4 was 2 mg/mL, the encapsulation efficiency was the highest (77%), while the change of loading efficiency (~1.3%) was very small (Figure S5). The particle size increased with the increase in Fe_3O_4 concentration, and PDI was relatively small when the concentration was 2 mg/mL. The concentration of Fe_3O_4 had an insignificant effect on the ζ-potential. The final ratios between Cur, CuS, and Fe_3O_4 in the nanoparticles were kept at 25:2:1.3.

The particle size of gelatin NPs functionalized with folic acid (FA-GNPs) was about 100 nm (Figure 2a). Encapsulation of Cur into the FA-GNPs increased the NP size to 120 ± 10 nm (Figure S3c). As shown in Figures S4c and S6, the size of gelatin NPs loaded with CuS NPs (CuS@GNPs-FA) was in the range of 160−240 nm, and the overall solution was pale green due to the presence of CuS NPs. The solution of gelatin NPs loaded with Fe_3O_4 NPs and CuS NPs (Fe_3O_4/CuS@GNPs-FA) showed an overall brown color, and the particle size increased further (Figure S6). The gelatin NPs loaded with curcumin, Fe_3O_4, and CuS NPs (Cur/Fe_3O_4/CuS@GNPs-FA) had a darker overall color and a yellowish-brown solution color in the presence of curcumin, and the size was within the range of 180 ± 15 nm (Figure 2b). The morphology of Fe_3O_4/CuS/Cur@GNPs-FA, as examined by TEM, is shown in Figure 2c. The particles had a narrow size distribution, which was consistent with the results obtained by DLS.

3.6. *In Vitro* Release and Stability of the Drug-Loaded Gelatin NPs. Figure 2d shows the release profiles of Fe_3O_4/CuS/Cur@GNPs-FA in PBS containing 20% EtOH and Tween-80 at pH 7.4 and pH 5.5. The addition of ethanol and Tween-80 increased the solubility of hydrophobic drugs.[38]

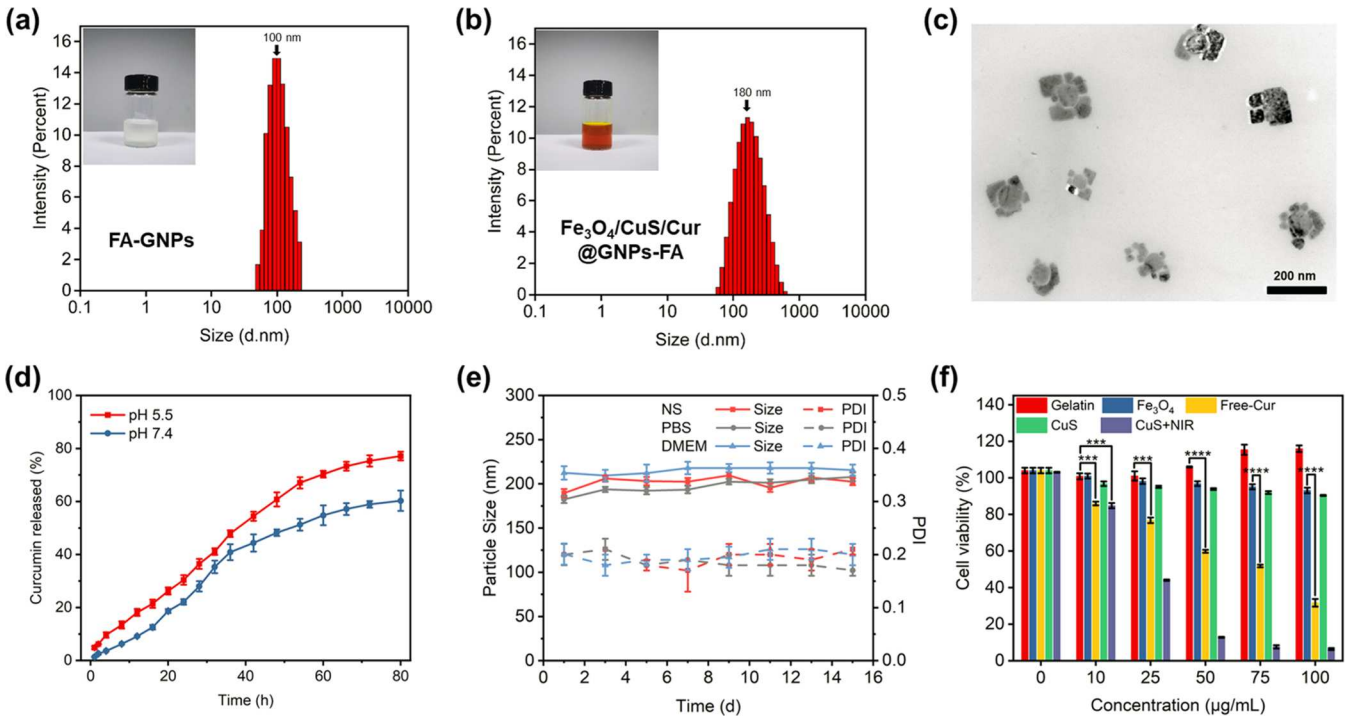

Figure 2. (a) Size distribution of gelatin nanoparticles functionalized with folic acid. (b) Size distribution of Fe_3O_4/CuS/Cur@GNPs-FA. (c) TEM of Fe_3O_4/CuS/Cur@GNPs-FA. (d) Drug release profiles of Fe_3O_4/CuS/Cur@GNPs-FA in PBS at pH 7.4 and 5.5 for 80 h. (e) Stability of drug-loaded gelatin nanoparticles in NS (0.9% NaCl), PBS, and DMEM at pH 7.4. (f) Cytotoxicity of blank gelatin nanoparticles, Fe_3O_4, free curcumin, CuS nanoparticles, and CuS + NIR on HFF-1 cells.

https://doi.org/10.1021/acsbiomaterials.3c00318
ACS Biomater. Sci. Eng. 2023, 9, 3402−3413

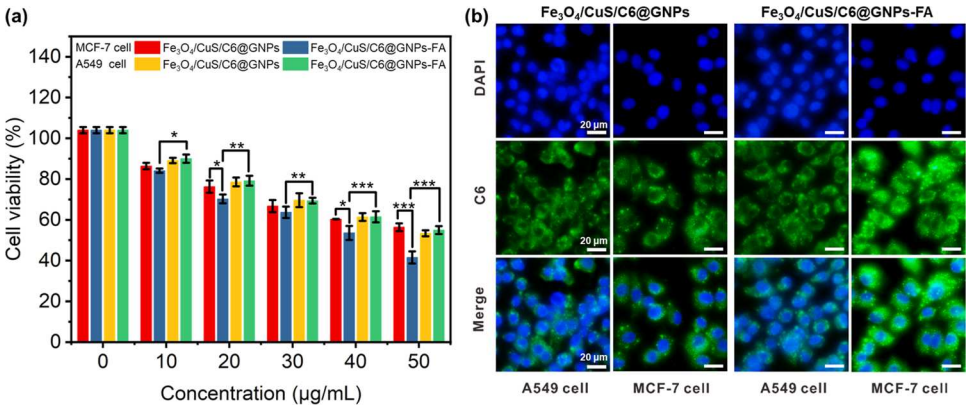

Figure 3. Co-culture of MCF-7 cells and A549 cells demonstrated the targeting effect of folic acid. Cell viability (a) and cellular uptake (b) of MCF-7 and A549 cells incubated with the nonfunctionalized and FA-functionalized GNPs.

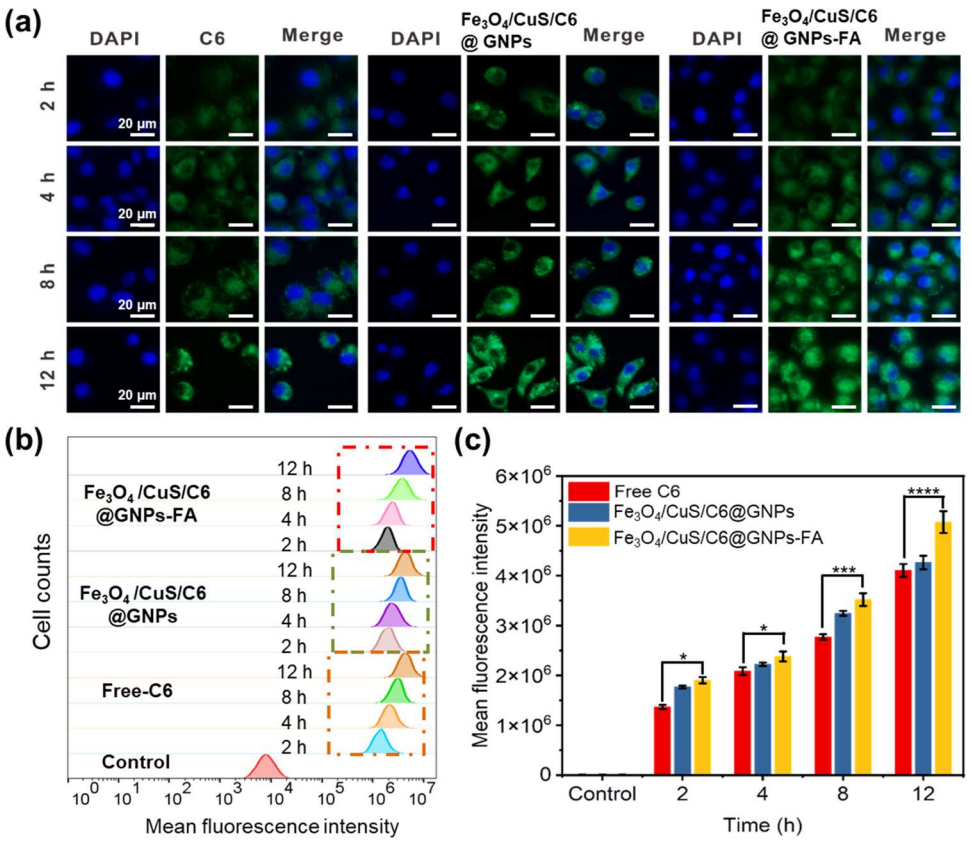

Figure 4. (a) Cellular uptake of NPs by MCF-7 cells. (b) FACS data of C6 fluorescence intensity. (c) Quantitative analysis of drug retention as measured with FACS. The final C6 concentration was controlled at 1 μg/mL.

As can be seen from the figure, the pH of the release medium affects the rate of curcumin release from gelatin NPs. When the pH was 7.4, the gelatin NPs released curcumin slowly. It took 40 h at pH 5.5 and 58 h at pH 7.4 for the release of curcumin from Fe_3O_4/CuS/Cur@GNPs-FA to reach 50%. It is known from the literature[62,69] that under acidic conditions, the gelatin structure relaxes, resulting in changes in the secondary structure of the protein, as a result of which the drug release of Fe_3O_4/CuS/Cur@GNPs-FA was promoted at pH 5.5.

To assess the stability of gelatin NPs, the particle size and PDI were measured in PBS (pH 7.4), NS (0.9% NaCl), and DMEM at 4 °C for 15 days (Figure 2e). There were no significant changes in particle size (200 nm), whereas a small fluctuation of PDI (predominantly around 0.2) was observed over 15 days, indicating that gelatin NPs were stable at the physiological condition and thus potent for the delivery of antitumor drugs.

3.7. Targeting Effect of the Folic Acid-Modified Gelatin NPs. MCF-7 cells and A549 cells were co-cultured to test the targeting effect of folic acid (Figure 3a). In order to better observe the uptake effect of different cells on gelatin nanoparticles, coumarin C6 with green fluorescence was used instead of curcumin. According to the literature, folate-grafted nanoparticles were easier to enter MCF-7 cells than A549 cells.[70] Both Fe_3O_4/CuS/Cur@GNPs and Fe_3O_4/CuS/Cur@GNPs-FA showed a concentration-dependent inhibition effect

https://doi.org/10.1021/acsbiomaterials.3c00318
ACS Biomater. Sci. Eng. 2023, 9, 3402−3413

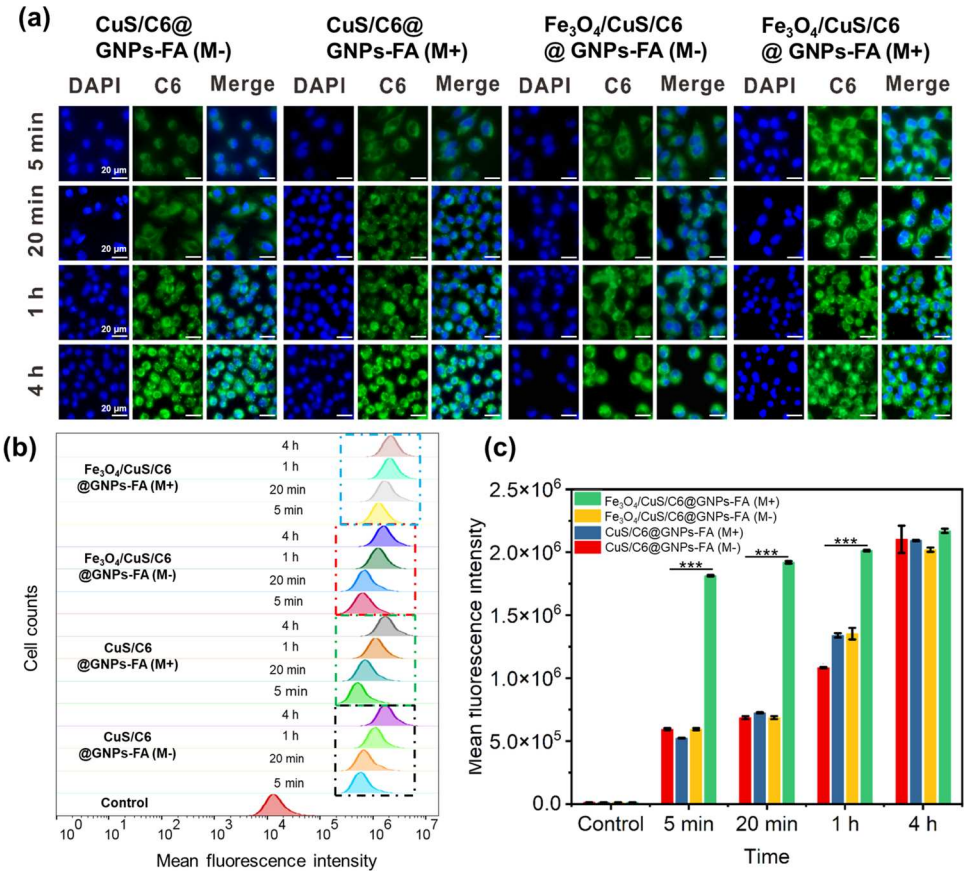

Figure 5. Comparison of the effect of absence and presence of a guiding external magnetic field on (a) GNP uptake by MCF-7 cells; (b) C6 fluorescence intensity as observed in FACS data; and (c) drug retention as measured by quantitative analysis of FACS data. The final C6 concentration was controlled at 1 μg/mL.

on MCF-7 and A549 cells. For MCF-7 cells at the same concentration, the cell inhibition rate of the Fe_3O_4/CuS/Cur@GNPs-FA group was higher than that of Fe_3O_4/CuS/Cur@GNPs. For A549 cells, the cell inhibition effect of the two drug-loaded gelatin NPs was similar. This indicates that Fe_3O_4/CuS/Cur@GNPs-FA has a clear folic acid targeting effect. Figure 3b shows the results of drug uptake on the co-culture of MCF-7 and A549 cells. The fluorescence intensity of MCF-7 cells in the Fe_3O_4/CuS/C6@GNPs-FA group was the brightest, while that of other groups was similar, indicating that folate-functionalized gelatin NPs can accelerate the drug intake and accumulation in folate receptor-positive cells through folate receptor-mediated endocytosis, while A549, a folate receptor-negative cell, has no such function. This result indicates that the folate-modified targeted gelatin NPs have a significantly stronger ability to induce apoptosis than non-targeted gelatin NPs.

3.8. *In Vitro* Cellular Uptake. The qualitative results of the NP uptake by MCF-7 cells, as observed under an inverted wide-field fluorescence microscope, are shown in Figure 4. The time of NP administration also had a significant effect on the NP uptake by MCF-7 cells. The fluorescence intensity of MCF-7 cells treated with Fe_3O_4/CuS/C6@GNPs-FA increased as the incubation time increased from 1 to 12 h, indicating that the cellular uptake of gelatin NPs was time-dependent. During the same post-administration incubation time, a stronger green fluorescence signal could be observed in the MCF-7 cells of the Fe_3O_4/CuS/C6@GNPs-FA group when compared against the coumarin C6 group and the Fe_3O_4/CuS/C6@GNPs group. This is because the surface of MCF-7 cells contains folate receptors, allowing the Fe_3O_4/CuS/C6@GNPs-FA to quickly enter cells through the folate receptor-mediated endocytosis. Coumarin C6 is a small fat-soluble molecule, almost insoluble in water, can only enter cells by passive diffusion and also gets easily excreted out of the cells, whereas gelatin NPs enter cells mainly through endocytosis.[71]

Further, flow cytometry was used to quantify the differences in cellular uptake of free coumarin C6, Fe_3O_4/CuS/C6@GNPs, and Fe_3O_4/CuS/C6@GNPs-FA (Figure 4b,c). The relative fluorescence values showed that the cellular uptake of Fe3O4/CuS/C6@GNPs-FA was significantly higher than that of free Coumarin C6, which was consistent with the results of fluorescence microscopy. CuS/C6@GNPs-FA and Fe_3O_4/CuS/C6@GNPs-FA with the applied external magnetic field (CuS/C6@GNPs(M+), Fe_3O_4/CuS/C6@GNPs-FA(M+)) and without the external magnetic field (CuS/C6@GNPs-FA(M−), Fe_3O_4/CuS/C6@GNPs-FA(M−)) were co-cultured with MCF-7 cells for 5 min, 20 min, 1 h, and 4 h, respectively. The results of the MCF-7 cellular uptake, as observed under an inverted confocal fluorescence microscope, are shown in Figure 5a. The fluorescence intensity of the four groups of MCF-7 cells increased with the incubation time, indicating that the cellular uptake of gelatin NPs was time-dependent. Within the same postadministration incubation time, the CuS/C6@GNPs(M+), CuS/C6@GNPs(M−), and Fe_3O_4/CuS/C6@GNPs-FA(M−) groups exhibited similar green fluorescence intensities in MCF-7 cells at 5 min, 20 min, and 1 h. The

https://doi.org/10.1021/acsbiomaterials.3c00318
ACS Biomater. Sci. Eng. 2023, 9, 3402−3413

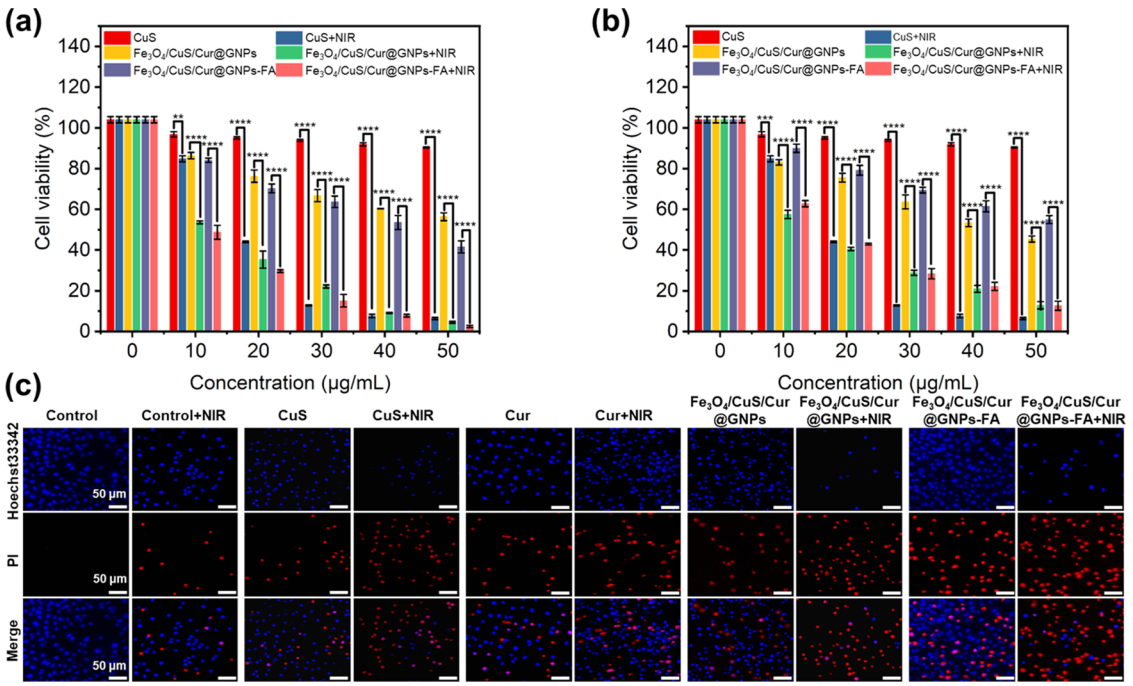

Figure 6. Cytotoxicity of different concentrations of pharmaceutical formulations to MCF-7 cells (a) and A549 cells (b) under NIR light. ($n \geq 3$;NIR,1.0 W/cm^2; ****$P < 0.0001$; ***$P < 0.001$; **$P < 0.01$; and *$P < 0.05$). (c) Live/dead staining of MCF-7 cells, where blue- and red-dyed cells represent live and dead cells at 24 h, respectively.

Fe_3O_4/CuS/C6@GNPs-FA(M+) group exhibited significantly stronger fluorescence intensity than the first three groups. At 4 h, more intense green fluorescence signals could be observed in the four groups of MCF-7 cells with little difference in intensity. The above results indicate that Fe_3O_4 can be guided by an external magnetic field to target gelatin NPs and accelerate the uptake of drugs by MCF-7, and reduce the treatment time of tumors. Flow cytometry was further used to quantify the difference in cellular uptake (Figure 5b,c). The relative fluorescence values indicated that the cellular uptake of Fe_3O_4/CuS/C6@GNPs-FA(M+) was faster than that of other groups, which was consistent with the fluorescence microscopy results.

3.9. Cytotoxicity of Gelatin NPs and Their Constituents. To test the cytocompatibility of materials and drug formulations, the viability of HFF-1 cells was assessed using the MTT assay. As shown in Figure 2f, after the blank gelatin NPs were co-cultured with HFF-1 cells for 24 h, the cell viability still reached 100%. This is because gelatin is a high-temperature hydrolyzed product of animal collagen, which is nontoxic and harmless to cells. There was even a weak cell-growth promotion effect, indicating that the blank gelatin NPs have good biocompatibility and can be used as safe carriers for antitumor drugs. Fe_3O_4 and CuS NPs were co-cultured with cells at concentrations of 10−100 μg/mL. After 24 h of culture, the cell survival rates were over 95 and 93%, respectively, indicating that Fe_3O_4 and CuS NPs could not induce apoptosis under normal conditions, while CuS NPs had a significant inhibitory effect on HFF-1 cells after NIR irradiation. The free anticancer drug curcumin had a clear inhibitory effect on HFF-1 cells.

The targeting effect of folic acid was examined by using MCF-7 cells and A549 cells. As shown in Figure 6a,b, the inhibitory effects of Fe_3O_4/CuS/Cur@GNPs and Fe_3O_4/CuS/Cur@GNPs-FA on MCF-7 cells and A549 cells were concentration-dependent. With the increase in concentration, the two groups of drug-loaded NPs had a stronger inhibitory effect on cells. For A549 cells, the cytostatic effects of the two drug-loaded gelatin NPs were comparable. In contrast, the inhibition rate of the Fe_3O_4/CuS/Cur@GNPs-FA group on MCF-7 cells was greater than that on A549 cells, indicating that CuS/Cur@GNPs-FA had a clear folic acid-mediated cell-targeting effect.

The effect of NIR irradiation on the cell viability of MCF-7 cells and A549 cells was determined by setting up two experiments with and without NIR irradiation. It can be seen from Figure 6a,b that the inhibition rates of the Fe_3O_4/CuS/Cur@GNPs group and the Fe_3O_4/CuS/Cur@GNPs-FA group with irradiation on MCF-7 cells and A549 cells were much higher than those in the nonirradiated group. The photothermal heating of irradiated CuS NPs enhanced tumor cell-killing ability. Fe_3O_4/CuS/Cur@GNPs-FA+NIR had a higher inhibition rate on MCF-7 cells due to folic acid-mediated targeting and photothermal ablation by irradiated CuS.

CuS NPs, Fe_3O_4/CuS/Cur@GNPs, and Fe_3O_4/CuS/Cur@GNPs-FA were incubated with MCF-7 cells for 24 h. The cells were irradiated with and without NIR before being stained with Hoechst 33,342 and PI to evaluate the killing of tumor cells by gelatin NPs (Figure 6c). It can be seen from the images that the killing efficiency of the four groups of agents on cells is in this order: Fe_3O_4/CuS/Cur@GNPs-FA > Fe_3O_4/CuS/Cur@GNPs > Cur > CuS. This indicates that folic acid has a targeting effect on MCF-7 cells, and therefore, the intake of Fe_3O_4/CuS/Cur@GNPs-FA by MCF-7 is higher than that of other groups, and thus the killing effect is stronger. After irradiation with near-infrared light, the order of cell-killing effect of each group from strong to weak was: Fe_3O_4/CuS/Cur@GNPs-FA > CuS > Fe_3O_4/CuS/Cur@GNPs > Cur. The reason behind the killing effect of CuS being stronger than that of Fe_3O_4/CuS/Cur@GNPs can be speculated that the layers of

https://doi.org/10.1021/acsbiomaterials.3c00318
ACS Biomater. Sci. Eng. 2023, 9, 3402−3413

gelatin on CuS cause a slow rate of photothermal heating of encapsulated CuS upon irradiation compared to free CuS. The red fluorescence (dead cells) in the same group increased significantly after NIR irradiation, except for curcumin, which had no photothermal effect. The blue fluorescence (live cells) of the Fe_3O_4/CuS/Cur@GNPs-FA + NIR group was only around 5%. It can be seen that with folic acid-mediated targeting and NIR irradiation, Fe_3O_4/CuS/Cur@GNPs-FA had an enhanced killing effect on MCF-7 cells, which is consistent with the conclusion of the MTT experiment.

4. CONCLUSIONS

In summary, we have successfully used a new swirl mixer to fabricate CuS, Fe_3O_4, and curcumin-encapsulated gelatin NPs in one step. Through the exploration of the total flow rate, the flow rate ratio, gelatin concentration, and the antisolvent, the gelatin NPs with desired properties were successfully prepared under optimal conditions. The size of the prepared gelatin NPs was within 200 nm with a small PDI (<0.1), and the NPs remained stable for over 2 weeks. The NP surface functionalization with folic acid enhanced the cellular uptake of the NPs into the MCF-7 cells. The encapsulation of Fe_3O_4 into the gelatin NPs also accelerated the cellular uptake of the NPs with a guiding external magnetic field. The photothermal heating of CuS NPs, together with the anticancer effect of curcumin, synergistically killed the MCF-7 breast cancer cells, with the highest killing efficiency of 95%. The experiments proved that the microfluidic preparation of gelatin NPs can well achieve the targeted delivery of anticancer drugs. It is believed that a microfluidic swirl mixer can be used in the pharmaceutical industry for the large-scale preparation of nanodrug delivery systems and will play a key role in the field of anticancer therapy.

■ ASSOCIATED CONTENT

Supporting Information

The Supporting Information is available free of charge at https://pubs.acs.org/doi/10.1021/acsbiomaterials.3c00318.

FIIR and ^{1}H NMR spectra data (Figure S1); characterization of Fe_3O_4 nanoparticles (Figure S2); curcumin encapsulation data (Figure S3); CuS encapsulation data (Figure S4); Fe_3O_4 encapsulation data (Figure S5); size distribution of CuS@GNPs-FA and Fe_3O_4/CuS@GNPs-FA (Figure S6) (PDF)

■ AUTHOR INFORMATION

Corresponding Author

Xiubo Zhao − *School of Pharmacy, Changzhou University, Changzhou 213164, China; Department of Chemical and Biological Engineering, University of Sheffield, Sheffield S1 3JD, U.K.;* orcid.org/0000-0002-4620-2893; Email: xiubo.zhao@cczu.edu.cn

Authors

Yu Xia − *School of Pharmacy, Changzhou University, Changzhou 213164, China*

Ruicheng Xu − *School of Pharmacy, Changzhou University, Changzhou 213164, China*

Siyuan Ye − *School of Pharmacy, Changzhou University, Changzhou 213164, China*

Jiaxuan Yan − *School of Pharmacy, Changzhou University, Changzhou 213164, China*

Piyush Kumar − *Department of Chemical and Biological Engineering, University of Sheffield, Sheffield S1 3JD, U.K.;* orcid.org/0000-0002-9965-8691

Peng Zhang − *School of Materials Science and Engineering, Changzhou University, Changzhou 213164, China*

Complete contact information is available at: https://pubs.acs.org/10.1021/acsbiomaterials.3c00318

Author Contributions

‖Y.X. and R.X. contributed equally to this work. Y.X.: methodology, validation, formal analysis, investigation, data curation, visualization, and writing—original draft. R.X. and S.Y.: methodology, validation, formal analysis, investigation, data curation, and visualization. J.Y.: methodology. P.K.: writing—review & editing. P.Z.: methodology. X.Z.: conceptualization, methodology, resources, writing—review & editing, supervision, project administration, and funding acquisition.

Notes

The authors declare no competing financial interest.

■ ACKNOWLEDGMENTS

The authors would like to thank Jiangsu specially appointed professor program, the innovation project of postgraduate training in Jiangsu province (SJCX21_1238 2021), and the EPSRC (EP/N007174/1 and EP/N023579/1) for support.

■ REFERENCES

(1) Soerjomataram, I.; Bray, F. Planning for tomorrow: global cancer incidence and the role of prevention 2020-2070. *Nat. Rev. Clin. Oncol.* **2021**, *18*, 663−672.

(2) Tomeh, M. A.; Hadianamrei, R.; Zhao, X. A Review of Curcumin and Its Derivatives as Anticancer Agents. *Int. J. Mol. Sci.* **2019**, *20*, No. 1033.

(3) Pan, F.; Li, Y.; Ding, Y.; Lv, S.; You, R.; Hadianamrei, R.; Tomeh, M. A.; Zhao, X. Anticancer effect of rationally designed alpha-helical amphiphilic peptides. *Colloids Surf., B* **2022**, *220*, No. 112841.

(4) Kenny, R. G.; Marmion, C. J. Toward Multi-Targeted Platinum and Ruthenium Drugs-A New Paradigm in Cancer Drug Treatment Regimens? *Chem. Rev.* **2019**, *119*, 1058−1137.

(5) Mizutani, K.; Kawakami, K.; Fujita, Y.; Kato, T.; Takai, M.; Kato, D.; Iinuma, K.; Koie, T.; Ito, M. Gene therapy of prostate cancer using liposomes containing perforin expression vector driven by the promoter of prostate-specific antigen gene. *Sci. Rep.* **2022**, *12*, No. 1442.

(6) Cirillo, S.; Tomeh, M. A.; Wilkinson, R. N.; Hill, C.; Brown, S.; Zhao, X. B. Designed Antitumor Peptide for Targeted siRNA Delivery into Cancer Spheroids. *ACS Appl. Mater. Interfaces* **2021**, *13*, 49713−49728.

(7) Norberg, S. M.; Hinrichs, C. S. Advances in Adoptive Cell Therapy for Head and Neck Cancer. *Otolaryngol. Clin. North Am.* **2021**, *54*, 761−768.

(8) Qu, J. J.; Mei, Q. H.; Chen, L. J.; Zhou, J. Y. Chimeric antigen receptor (CAR)-T-cell therapy in non-small-cell lung cancer (NSCLC): current status and future perspectives. *Cancer Immunol., Immunother.* **2021**, *70*, 619−631.

(9) Huang, Y. J.; Guan, Z. L.; Dai, X. L.; Shen, Y. F.; Wei, Q.; Ren, L. L.; Jiang, J. W.; Xiao, Z. H.; Jiang, Y. L.; Liu, D.; Huang, Z. Q.; Xu, X. Y.; Luo, Y.; Zhao, C. S. Engineered macrophages as near-infrared light activated drug vectors for chemo-photodynamic therapy of primary and bone metastatic breast cancer. *Nat. Commun.* **2021**, *12*, No. 4310.

(10) Nakayama, T.; Sano, T.; Oshimo, Y.; Kawada, C.; Kasai, M.; Yamamoto, S.; Fukuhara, H.; Inoue, K.; Ogura, S. Enhanced lipid metabolism induces the sensitivity of dormant cancer cells to 5-

aminolevulinic acid-based photodynamic therapy. *Sci. Rep.* **2021**, *11*, No. 7290.
(11) Qin, X.; Wu, C.; Niu, D. C.; Qin, L. M.; Wang, X.; Wang, Q. G.; Li, Y. S. Peroxisome inspired hybrid enzyme nanogels for chemodynamic and photodynamic therapy. *Nat. Commun.* **2021**, *12*, No. 5243.
(12) Hu, K.; Xie, L.; Zhang, Y. D.; Hanyu, M.; Yang, Z. M.; Nagatsu, K.; Suzuki, H.; Ouyang, J.; Ji, X. Y.; Wei, J. J.; Xu, H.; Farokhzad, O. C.; Liang, S. H.; Wang, L.; Tao, W.; Zhang, M. R. Marriage of black phosphorus and Cu2+ as effective photothermal agents for PET-guided combination cancer therapy. *Nat. Commun.* **2020**, *11*, No. 2778.
(13) Liu, F.; Wang, X. D.; Du, S. Y. Production of gold/silver doped carbon nanocomposites for effective photothermal therapy of colon cancer. *Sci. Rep.* **2020**, *10*, No. 7618.
(14) Sharifi, M.; Hasan, A.; Nanakali, N. M. Q.; Salihi, A.; Qadir, F. A.; Muhammad, H. A.; Shekha, M. S.; Aziz, F. M.; Amen, K. M.; Najafi, F.; Yousefi-Manesh, H.; Falahati, M. Combined chemo-magnetic field-photothermal breast cancer therapy based on porous magnetite nanospheres. *Sci. Rep.* **2020**, *10*, No. 5925.
(15) Zhao, H. S.; Liu, Z. W.; Wei, Y.; Zhang, L.; Wang, Z.; Ren, J. S.; Qu, X. G. NIR-II Light Leveraged Dual Drug Synthesis for Orthotopic Combination Therapy. *ACS Nano* **2022**, *16*, 20353−20363.
(16) Huang, W.; Zhang, J.; Luo, L.; Yu, Y.; Sun, T. L. Nitric Oxide and Tumors: From Small-Molecule Donor to Combination Therapy. *Acs Biomater. Sci. Eng.* **2023**, *9*, 139−152.
(17) Zhang, Q. H.; Zhang, J. M.; Song, J.; Liu, Y. Z.; Ren, X. Z.; Zhao, Y. L. Protein-Based Nanomedicine for Therapeutic Benefits of Cancer. *ACS Nano* **2021**, *15*, 8001−8038.
(18) Youden, B.; Jiang, R.; Carrier, A. J.; Servos, M. R.; Zhang, X. A Nanomedicine Structure-Activity Framework for Research, Development, and Regulation of Future Cancer Therapies. *ACS Nano* **2022**, *16*, 17497−17551.
(19) Zhang, B.; Shao, C. W.; Zhou, K. M.; Li, Q.; Duan, Y. T.; Yang, Y. S.; Zhu, H. L. A NIR-triggered multifunctional nanoplatform mediated by Hsp70 siRNA for chemo-hypothermal photothermal synergistic therapy. *Biomater. Sci.* **2021**, *9*, 6501−6509.
(20) Jeong, W. Y.; Kwon, M.; Choi, H. E.; Kim, K. S. Recent advances in transdermal drug delivery systems: a review. *Biomater. Res.* **2021**, *25*, No. 24.
(21) Tomeh, M. A.; Hadianamrei, R.; Zhao, X. Silk Fibroin as a Functional Biomaterial for Drug and Gene Delivery. *Pharmaceutics* **2019**, *11*, No. 494.
(22) Aslam, H.; Shukrullah, S.; Naz, M. Y.; Fatima, H.; Hussain, H.; Ullah, S.; Assiri, M. A. Current and future perspectives of multifunctional magnetic nanoparticles based controlled drug delivery systems. *J. Drug Delivery Sci. Technol.* **2022**, *67*, No. 102946.
(23) Tomeh, M. A.; Hadianamrei, R.; Sun, W.; Xu, D.; Brown, S.; Zhao, X. Stiffness-tuneable nanocarriers for controlled delivery of ASC-J9 into colorectal cancer cells. *J. Colloid Interface Sci.* **2021**, *594*, 513−521.
(24) Tomeh, M. A.; Mansor, M. H.; Hadianamrei, R.; Sun, W.; Zhao, X. Optimization of large-scale manufacturing of biopolymeric and lipid nanoparticles using microfluidic swirl mixers. *Int. J. Pharm.* **2022**, *620*, No. 121762.
(25) Jin, Y.; Tomeh, M. A.; Zhang, P.; Su, M.; Zhao, X.; Cai, Z. Microfluidic fabrication of photo-responsive Ansamitocin P-3 loaded liposomes for the treatment of breast cancer. *Nanoscale* **2023**, *15*, 3780−3795.
(26) Song, W.; Su, X.; Gregory, D. A.; Li, W.; Cai, Z.; Zhao, X. Magnetic Alginate/Chitosan Nanoparticles for Targeted Delivery of Curcumin into Human Breast Cancer Cells. *Nanomaterials* **2018**, *8*, No. 907.
(27) Lazarus, L. L.; Riche, C. T.; Marin, B. C.; Gupta, M.; Malmstadt, N.; Brutchey, R. L. Two-Phase Microfluidic Droplet Flows of Ionic Liquids for the Synthesis of Gold and Silver Nanoparticles. *ACS Appl. Mater. Interfaces* **2012**, *4*, 3077−3083.
(28) Shao, K.; Singha, S.; Clemente-Casares, X.; Tsai, S.; Yang, Y.; Santamaria, P. Nanoparticle-based immunotherapy for cancer. *ACS Nano* **2015**, *9*, 16−30.
(29) Tomeh, M. A.; Hadianamrei, R.; Xu, D.; Brown, S.; Zhao, X. Peptide-functionalised magnetic silk nanoparticles produced by a swirl mixer for enhanced anticancer activity of ASC-J9. *Colloids Surf., B* **2022**, *216*, No. 112549.
(30) Song, W.; Gregory, D. A.; Al-Janabi, H.; Muthana, M.; Cai, Z.; Zhao, X. Magnetic-silk/polyethyleneimine core-shell nanoparticles for targeted gene delivery into human breast cancer cells. *Int. J. Pharm.* **2019**, *555*, 322−336.
(31) Wang, X.; Hou, M.; Liu, X.; Yue, O.; Zheng, M. Feasibility Study of Gelatin Preparation from the Bioinspired Collagen Aggregates by a "Two-step" Facile Degradation Method. *ACS Appl. Bio Mater.* **2021**, *4*, 2363−2372.
(32) Wong, P. T.; Choi, S. K. Mechanisms of Drug Release in Nanotherapeutic Delivery Systems. *Chem. Rev.* **2015**, *115*, 3388−3432.
(33) Hou, S.; Mahadevegowda, S. H.; Mai, V. C.; Chan-Park, M. B.; Duan, H. W. Glycosylated Copper Sulfide Nanocrystals for Targeted Photokilling of Bacteria in the Near-Infrared II Window. *Adv. Ther.* **2019**, *2*, No. 1900052.
(34) Tomeh, M. A.; Zhao, X. Recent Advances in Microfluidics for the Preparation of Drug and Gene Delivery Systems. *Mol. Pharm.* **2020**, *17*, 4421−4434.
(35) Qiu, J.; Tomeh, M. A.; Jin, Y.; Zhang, B.; Zhao, X. Microfluidic formulation of anticancer peptide loaded ZIF-8 nanoparticles for the treatment of breast cancer. *J. Colloid Interface Sci.* **2023**, *642*, 810−819.
(36) Shepherd, S. J.; Issadore, D.; Mitchell, M. J. Microfluidic formulation of nanoparticles for biomedical applications. *Biomaterials* **2021**, *274*, No. 120826.
(37) Song, W. X.; Muthana, M.; Mukherjee, J.; Falconer, R. J.; Biggs, C. A.; Zhao, X. B. Magnetic-Silk Core-Shell Nanoparticles as Potential Carriers for Targeted Delivery of Curcumin into Human Breast Cancer Cells. *Acs Biomater. Sci. Eng.* **2017**, *3*, 1027−1038.
(38) Xu, R. C.; Tomeh, M. A.; Ye, S. Y.; Zhang, P.; Lv, S. W.; You, R. R.; Wang, N.; Zhao, X. B. Novel microfluidic swirl mixers for scalable formulation of curcumin loaded liposomes for cancer therapy. *Int. J. Pharm.* **2022**, *622*, No. 121857.
(39) Lv, S. W.; Jing, R.; Liu, X. W.; Shi, H. L.; Shi, Y. F.; Wang, X. G.; Zhao, X. B.; Cao, K.; Lv, Z. One-Step Microfluidic Fabrication of Multi-Responsive Liposomes for Targeted Delivery of Doxorubicin Synergism with Photothermal Effect. *Int. J. Nanomed.* **2021**, *16*, 7759−7772.
(40) Hsu, H. L.; Chen, J. P. Preparation of thermosensitive magnetic liposome encapsulated recombinant tissue plasminogen activator for targeted thrombolysis. *J. Magn. Magn. Mater.* **2017**, *427*, 188−194.
(41) Huang, L. J.; He, M.; Chen, B. B.; Hu, B. A designable magnetic MOF composite and facile coordination-based post-synthetic strategy for the enhanced removal of Hg2+ from water. *J. Mater. Chem. A* **2015**, *3*, 11587−11595.
(42) Zhang, Y.; Li, J. S.; Lang, M. D.; Tang, X. L.; Li, L.; Shen, X. Z. Folate-functionalized nanoparticles for controlled 5-Fluorouracil delivery. *J. Colloid Interface Sci.* **2011**, *354*, 202−209.
(43) Zhao, X. W.; Zhang, J. L.; Shi, L. H.; Xian, M.; Dong, C.; Shuang, S. M. Folic acid-conjugated carbon dots as green fluorescent probes based on cellular targeting imaging for recognizing cancer cells. *RSC Adv.* **2017**, *7*, 42159−42167.
(44) Xu, R.; Tomeh, M. A.; Ye, S.; Zhang, P.; Lv, S.; You, R.; Wang, N.; Zhao, X. Novel microfluidic swirl mixers for scalable formulation of curcumin loaded liposomes for cancer therapy. *Int. J. Pharm.* **2022**, *622*, No. 121857.
(45) Lee, J. J.; Lee, S. Y.; Park, J. H.; Kim, D. D.; Cho, H. J. Cholesterol-modified poly(lactide-co-glycolide) nanoparticles for tumor-targeted drug delivery. *Int. J. Pharm.* **2016**, *509*, 483−491.
(46) Qi, C. P.; Wang, D.; Gong, X.; Zhou, Q. Y.; Yue, X. X.; Li, C. L.; Li, Z. P.; Tian, G. X.; Zhang, B.; Wang, Q.; Wei, X. H.; Wu, J. L. Co-Delivery of Curcumin and Capsaicin by Dual-Targeting Lip-

https://doi.org/10.1021/acsbiomaterials.3c00318
ACS Biomater. Sci. Eng. 2023, 9, 3402−3413

osomes for Inhibition of aHSC-Induced Drug Resistance and Metastasis. *ACS Appl. Mater. Interfaces* **2021**, *13*, 16019−16035.
(47) Xu, C.; Liu, W.; Hu, Y.; Li, W. P.; Di, W. Bioinspired tumor-homing nanoplatform for co-delivery of paclitaxel and siRNA-E7 to HPV-related cervical malignancies for synergistic therapy. *Theranostics* **2020**, *10*, 3325−3339.
(48) Wang, Y. F.; Ren, J.; Liu, Y. H.; Liu, R.; Wang, L. L.; Yuan, Q. L.; He, J. M.; Nie, Y. M.; Xu, J.; Yu, J. M. Preparation and evaluation of folic acid modified succinylated gelatin micelles for targeted delivery of doxorubicin. *J. Drug Delivery Sci. Technol.* **2018**, *46*, 400−407.
(49) Stella, B.; Arpicco, S.; Peracchia, M. T.; Desmaele, D.; Hoebeke, J.; Renoir, M.; D'Angelo, J.; Cattel, L.; Couvreur, P. Design of folic acid-conjugated nanoparticles for drug targeting. *J. Pharm. Sci.* **2000**, *89*, 1452−1464.
(50) Kazi, J.; Mukhopadhyay, R.; Sen, R.; Jha, T.; Ganguly, S.; Debnath, M. C. Design of 5-fluorouracil (5-FU) loaded, folate conjugated peptide linked nanoparticles, a potential new drug carrier for selective targeting of tumor cells. *MedChemComm* **2019**, *10*, 559−572.
(51) Das, R. P.; Chakravarti, S.; Patel, S. S.; Lakhamje, P.; Gurjar, M.; Gota, V.; Singh, B. G.; Kunwar, A. Tuning the pharmacokinetics and efficacy of irinotecan (IRI) loaded gelatin nanoparticles through folate conjugation. *Int. J. Pharm.* **2020**, *586*, No. 119522.
(52) van Hoorick, J.; Gruber, P.; Markovic, M.; Tromayer, M.; Van Erps, J.; Thienpont, H.; Liska, R.; Ovsianikov, A.; Dubruel, P.; Van Vlierberghe, S. Cross-Linkable Gelatins with Superior Mechanical Properties Through Carboxylic Acid Modification: Increasing the Two-Photon Polymerization Potential. *Biomacromolecules* **2017**, *18*, 3260−3272.
(53) Wang, Z. F.; Tang, X. J.; Wang, X. X.; Yang, D. D.; Yang, C.; Lou, Y. B.; Chen, J. X.; He, N. Y. Near-infrared light-induced dissociation of zeolitic imidazole framework-8 (ZIF-8) with encapsulated CuS nanoparticles and their application as a therapeutic nanoplatform. *Chem. Commun.* **2016**, *52*, 12210−12213.
(54) Petcharoen, K.; Sirivat, A. Synthesis and characterization of magnetite nanoparticles via the chemical co-precipitation method. *Mater. Sci. Eng. B* **2012**, *177*, 421−427.
(55) Mohanty, B.; Bohidar, H. B. Systematic of alcohol-induced simple coacervation in aqueous gelatin solutions. *Biomacromolecules* **2003**, *4*, 1080−1086.
(56) Famta, P.; Shah, S. R.; Fernandes, V.; Kumar, K. C.; Bagasariya, D.; Samim, K. S.; Khatri, D. K.; Singh, S. B.; Srivastava, S. Quality by design (QbD) assisted Fabrication & evaluation of Simvastatin loaded Nano-Enabled thermogel for melanoma therapy. *Int. J. Pharm.* **2022**, *628*, No. 122270.
(57) Xue, J.; Zhong, Q. Blending lecithin and gelatin improves the formation of thymol nanodispersions. *J. Agric. Food Chem.* **2014**, *62*, 2956−2962.
(58) Kim, B.; Han, S. W.; Choi, S. E.; Yim, D.; Kim, J. H.; Wyss, H. M.; Kim, J. W. Monodisperse Microshell Structured Gelatin Microparticles for Temporary Chemoembolization. *Biomacromolecules* **2018**, *19*, 386−391.
(59) Saravanan, M.; Bhaskar, K.; Maharajan, G.; Pillai, K. S. Ultrasonically controlled release and targeted delivery of diclofenac sodium via gelatin magnetic microspheres. *Int. J. Pharm.* **2004**, *283*, 71−82.
(60) Annamalai, R. T.; Turner, P. A.; Carson, W. F.; Levi, B.; Kunkel, S.; Stegemann, J. P. Harnessing macrophage-mediated degradation of gelatin microspheres for spatiotemporal control of BMP2 release. *Biomaterials* **2018**, *161*, 216−227.
(61) Leeuwenburgh, S. C. G.; Jo, J.; Wang, H. A.; Yamamoto, M.; Jansen, J. A.; Tabata, Y. Mineralization, Biodegradation, and Drug Release Behavior of Gelatin/Apatite Composite Microspheres for Bone Regeneration. *Biomacromolecules* **2010**, *11*, 2653−2659.
(62) Yang, J.; Zhou, M.; Li, W. D.; Lin, F.; Shan, G. Q. Preparation and Evaluation of Sustained Release Platelet-Rich Plasma-Loaded Gelatin Microspheres Using an Emulsion Method. *Acs Omega* **2020**, *5*, 27113−27118.
(63) Javanbakht, S.; Nezhad-Mokhtari, P.; Shaabani, A.; Arsalani, N.; Ghorbani, M. Incorporating Cu-based metal-organic framework/drug nanohybrids into gelatin microsphere for ibuprofen oral delivery. *Mater. Sci. Eng. C* **2019**, *96*, 302−309.
(64) Likitdecharoj, P.; Ratanavaraporn, J. Comparative study in physico-chemical properties of gelatin derivatives and their microspheres as carriers for controlled release of green tea's extract. *J. Drug Delivery Sci. Technol.* **2018**, *47*, 367−374.
(65) Tajima, S.; Tabata, Y. Preparation of EpH4 and 3T3L1 cells aggregates incorporating gelatin hydrogel microspheres for a cell condition improvement. *Regener. Ther.* **2017**, *6*, 90−99.
(66) Teng, S. H.; Wang, P. One-pot synthesis of HA-coated gelatin microspheres by an emulsion method. *Mater. Lett.* **2011**, *65*, 1348−1350.
(67) Chen, X. Y.; Fan, M.; Tan, H. P.; Ren, B. W.; Yuan, G. L.; Jia, Y.; Li, J. L.; Xiong, D. S.; Xing, X. D.; Niu, X. H.; Hu, X. H. Magnetic and self-healing chitosan-alginate hydrogel encapsulated gelatin microspheres via covalent cross-linking for drug delivery. *Mater. Sci. Eng. C* **2019**, *101*, 619−629.
(68) Gómez-Estaca, J.; Gavara, R.; Hernandez-Munoz, P. Encapsulation of curcumin in electrosprayed gelatin microspheres enhances its bioaccessibility and widens its uses in food applications. *Innovative Food Sci. Emerging Technol.* **2015**, *29*, 302−307.
(69) Zandi, M.; Mirzadeh, H.; Mayer, C. Effects of concentration, temperature, and pH on chain mobility of gelatin during the early stages of gelation. *Iran. Polym. J.* **2007**, *16*, 861−870.
(70) Wang, J.; Wang, Y.; Liu, Q.; Yang, L. N.; Zhu, R. R.; Yu, C. Z.; Wang, S. L. Rational Design of Multifunctional Dendritic Mesoporous Silica Nanoparticles to Load Curcumin and Enhance Efficacy for Breast Cancer Therapy. *ACS Appl. Mater. Interfaces* **2016**, *8*, 26511−26523.
(71) Qi, C.; Wang, D.; Gong, X.; Zhou, Q.; Yue, X.; Li, C.; Li, Z.; Tian, G.; Zhang, B.; Wang, Q.; Wei, X.; Wu, J. Co-Delivery of Curcumin and Capsaicin by Dual-Targeting Liposomes for Inhibition of aHSC-Induced Drug Resistance and Metastasis. *ACS Appl. Mater. Interfaces* **2021**, *13*, 16019−16035.

https://doi.org/10.1021/acsbiomaterials.3c00318
ACS Biomater. Sci. Eng. 2023, 9, 3402−3413